

## Direct observation of the giant dipole resonance of $^{16}\text{O}$ via electromagnetic dissociation

D. L. Olson, M. Baumgartner,\* D. E. Greiner, P. J. Lindstrom,  
T. J. M. Symons, R. Wada,† and M. L. Webb  
*Lawrence Berkeley Laboratory, Berkeley, California 94720*

B. L. Berman  
*Center for Nuclear Studies, The George Washington University, Washington, D.C. 20052*

H. J. Crawford and J. M. Engelage  
*University of California, Space Sciences Laboratory, Berkeley, California 94720*  
(Received 3 July 1991)

We have measured the invariant-mass spectrum of the final-state  $^{15}\text{N}+p$  system in the reaction  $T(^{16}\text{O}, ^{15}\text{N}+p)X$  at 2.1A GeV with Be, Cu, and U targets ( $T$ ). Electromagnetic dissociation of the  $^{16}\text{O}$  projectile nucleus in the Coulomb field of the target nucleus produces two prominent peaks in the proton-energy spectrum, one at 9 MeV, from transitions to the ground state of the residual  $^{15}\text{N}$  nucleus, and the other at 4 MeV, from transitions to excited states. This is corroborated by  $\gamma$  rays corresponding to the deexcitation of the  $^{15}\text{N}$  nucleus which are in coincidence with the 4-MeV peak and are suppressed for the 9-MeV peak. Nucleon-nucleus diffractive dissociation makes a significant contribution to the cross section and results in a peak at 1.5 MeV. Nucleon-nucleon quasielastic scattering results in a featureless high-energy tail above 20 MeV.

### I. INTRODUCTION

#### A. General

The electromagnetic dissociation (EMD) of relativistic heavy ions has been studied in inclusive-projectile [1–6], exclusive-projectile [7], and target-fragmentation [8] experiments. In these experiments, integrated EMD cross sections have been measured. Here we report the first measurement of an exclusive *differential* EMD cross section, via a two-particle coincidence experiment, which permits us to extract information about the EMD process in much greater detail. In this investigation we had two primary objectives: (1) to perform a rigorous test of our understanding of the EMD process and (2) to determine the feasibility of utilizing EMD for photonuclear-reaction studies of both stable and  $\beta$ -unstable nuclei.

Our choice of experimental parameters for meeting these objectives is a beam of  $^{16}\text{O}$  nuclei at 2.1A GeV initiating the reaction  $T(^{16}\text{O}, ^{15}\text{N}+p)X$  for targets ( $T$ ) of U, Cu, and Be. The  $^{16}\text{O}$  nucleus has an advantage over any other as a result of the detailed photonuclear studies which have been carried out previously for this nucleus by Caldwell *et al.* [9, 10]. The measured cross sections for decays to the  $^{15}\text{N}$  ground state,  $\sigma(\gamma, p_0)$  [11, 12], and to excited states of  $^{15}\text{N}_i$ ,  $\sigma(\gamma, p_i)$  [9, 10], enable us to make a precise prediction of the proton energy spectrum generated by the EMD process.

As an additional verification of the EMD process, we used a NaI detector array to measure the deexcitation  $\gamma$  rays from the  $^{15}\text{N}$  fragment. The EMD theory predicts

two peaks in the proton energy spectrum (as measured in the projectile rest frame). A peak at about 9 MeV proton energy results from decays of the giant dipole resonance (GDR) in  $^{16}\text{O}$  to the ground state of  $^{15}\text{N}$ , and a peak at about 4 MeV proton energy results from GDR decays to excited states at 5–6 MeV in  $^{15}\text{N}$ , which result in lower proton energies. These excited states in  $^{15}\text{N}$  decay by emission of a  $\gamma$  ray which is in coincidence with a 4-MeV proton.

#### B. Kinematics

A detailed description of EMD is given in Ref. [2]. In this discussion we utilize the notation of inverse kinematics, in which all of the kinematic variables are calculated in the rest frame of the projectile-fragment system. The basic idea is that the  $^{16}\text{O}$  projectile nucleus absorbs a virtual photon from the Coulomb field of the target nucleus. This virtual photon, which is nearly purely transverse, excites the  $^{16}\text{O}$  nucleus to a level with an energy equal to the virtual photon energy,  $\omega$ , which then decays into an  $^{15}\text{N}$  and a proton. The  $^{15}\text{N}$  is produced either in its ground state or in an excited state with excitation energy  $E_i$  which subsequently decays by emitting one or more  $\gamma$  rays.

By measuring the momentum of the projectile-frame charged particles we are able to reconstruct the invariant mass of the charged-particle final state,  $M$ . This is related to  $\omega$  by

$$M = |\mathcal{P}_p + \mathcal{P}_N| = M_O + \omega - E_i = M_N + M_p + E^* , \quad (1)$$

where  $M_O$ ,  $M_N$ , and  $M_p$  are the rest masses of  $^{16}\text{O}$ ,  $^{15}\text{N}$ , and the proton, respectively,  $\mathcal{P}_p$  and  $\mathcal{P}_N$  are the four-momenta of the proton and  $^{15}\text{N}$ , and  $E_i$  is the internal excitation energy of the  $^{15}\text{N}$ . The excitation energy of the final state  $^{15}\text{N}+p$  system is

$$E^* = \omega + Q - E_i, \quad (2)$$

where  $Q$  is the  $Q$  value for the reaction  $^{16}\text{O} \rightarrow ^{15}\text{N}+p$ .

The EMD cross section is calculated as the product of the virtual-photon spectrum,  $N_\gamma(\omega)$ , and one of the measured photoproton cross sections,  $\sigma(\gamma, p)$  [9–12],

$$\frac{d\sigma_{\text{em}}}{d\omega} = \sigma(\gamma, p)N_\gamma(\omega). \quad (3)$$

This is related to  $d\sigma/dE_p$  as

$$\begin{aligned} \frac{d\sigma}{dE_p} &= \sum_{i=0}^n \frac{d\sigma_{\text{em}}^i}{d\omega} \frac{d\omega}{dE_p} \\ &= \sum_{i=0}^n \sigma(\gamma, p_i)N_\gamma(\omega) \frac{d\omega}{dE_p}, \end{aligned} \quad (4)$$

where  $i$  denotes the state in  $^{15}\text{N}$ , and

$$\frac{d\omega}{dE_p} = \frac{M_N + M_p}{M_N} \approx \frac{16}{15} \quad (5)$$

in the nonrelativistic limit.  $E_p$  is the inverse-kinematics equivalent to the proton energy measured in a normal-kinematics experiment.

## II. EXPERIMENTAL SETUP AND ANALYSIS

This experiment was performed at the Lawrence Berkeley Laboratory (LBL) HISS facility. A complete description of this facility is given in Ref. [13]. A schematic diagram of the setup is shown in Fig. 1. The 2.14 GeV  $^{16}\text{O}$  beam is incident upon a set of plastic scintillation counters (TOF<sub>1</sub>, TOT, HS, E) and drift chambers (DC<sub>3</sub>, DC<sub>4</sub>) before entering the main vacuum tank of the HISS magnet and striking the target. The projectile fragments produced in the target continue on through the 1 m×2 m drift chambers and multislit time-of-flight (TOF) wall. A small 7.6 cm diam plastic scintillation counter (DS) is used to veto noninteracting beam particles. A 20 cm×40 cm plastic scintillator (NS) located just behind the TOF wall was used for the  $^{15}\text{N}$  trigger. The NS counter was located on the high-rigidity side of the beam and had a pulse-height threshold set at the mid-

dle of the carbon fragment peak. The NaI detector was a 7 by 7 array of rectangular parallelepipeds each measuring  $6.2 \times 6.2 \times 50 \text{ cm}^3$ . These were aligned with the long axis pointing at the target. Each element had one photomultiplier tube on the end away from the target.

A proton coincidence trigger, P, was made with a set of TOF wall slats in the region corresponding to the projectile-velocity protons. Signals from each photomultiplier tube at the top and bottom of the scintillator slat were fed into mean timers. The output signals of the mean timers were fed into a logic OR unit which gave a signal which indicated that one or more TOF slats fired from the region of interest. The primary trigger for this experiment was  $\text{TOT} \cdot \text{TOF}_1 \cdot E_{\text{lo}} \cdot \overline{E_{\text{hi}}} \cdot \overline{\text{HS}} \cdot \overline{\text{DS}} \cdot \text{NS} \cdot \text{P}$ . This requires that a beam particle be incident upon the target and that it interact before the DS scintillator and be in coincidence with the NS scintillator and with the proton-coincidence logic. The incident beam is counted as the number of particles satisfying the condition  $\text{TOT} \cdot \text{TOF}_1 \cdot E_{\text{lo}} \cdot \overline{E_{\text{hi}}} \cdot \overline{\text{HS}}$  that occurred during the live time of the data acquisition system [13].

The incident beam vector and position at the target is determined from DC<sub>3</sub> and DC<sub>4</sub>. The downstream particle tracks are determined by DC<sub>1</sub> and DC<sub>2</sub> and the charge is measured by pulse height in the TOF wall. The rigidity is determined from a knowledge of the magnetic field and the trajectory given by the drift chambers. Particle identification is determined by the rigidity and charge measurements. In this experiment, because we are focusing on fragments that are at low velocity in the beam rest frame, the rigidity distributions of the particles do not overlap significantly [14], so that time-of-flight information is not necessary for particle identification.

We collected proton-energy spectra for U, Cu, Be, and blank targets. For each of these spectra the reaction rate is calculated as  $R_t(E_p) = N_t(^{15}\text{N} + p, E_p)/B$ , where  $N_t(^{15}\text{N} + p, E_p)$  is the number of events with an  $^{15}\text{N}+p$  final state with proton energy  $E_p$  for the target  $t$ , and  $B$  is the number of beam particles incident upon the target. The net target-in rate is calculated as  $R'_t = R_t - R_{\text{blank}}$ .

The cross sections  $(d\sigma/dE_p)$ (mb/MeV) are calculated from the net rate as

$$\frac{d\sigma(t)}{dE_p} = \frac{R'_t A_t N_A}{f \rho_t d_t}, \quad (6)$$

where  $N_A$  is Avogadro's number and  $A_t$ ,  $f$ ,  $\rho_t$ , and  $d_t$  are the atomic weight, normalization factor, density, and thickness of the target, respectively. The differential cross sections  $d\sigma/dE_p$  for the U, Cu, and Be targets are shown in Fig. 2.

The normalization factor,  $f$ , accounts for the overall efficiency for reconstructing  $^{15}\text{N}+p$  events. We have chosen the value of  $f$  so that

$$\int_0^{30} \left( \frac{d\sigma(\text{U})}{dE_p} - \Gamma_{\text{U}} \frac{d\sigma(\text{Be})}{dE_p} \right) dE_p = \int \sigma(\gamma, p)N_\gamma(\omega)d\omega = 82 \text{ mb} \quad (7)$$

[see Eq. (3)], where the parameters for calculating  $N_\gamma(\omega)$  are taken from Ref. [2] and the photonuclear cross section

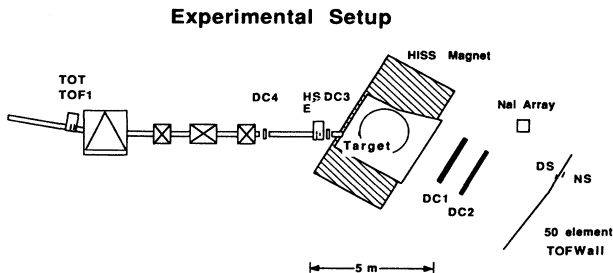


FIG. 1. A schematic view of the experimental setup.

$\sigma(\gamma, p)$  is from Refs. [9] and [10]. The scaling factor  $\Gamma_U$ , which accounts for the different radii of U and Be, is discussed below.

### III. RESULTS AND DISCUSSION

#### A. Cross sections

There are two distinct regions in these cross sections, as pointed out by Webb *et al.* [15], the peak structure for  $E_p < 20$  MeV and the smooth high-energy tail for  $E_p > 20$  MeV. The high-energy tail can be attributed to a quasifree nucleon-nucleon ( $N-N$ ) scattering process and is a significant part of single-nucleon knock-out reactions.

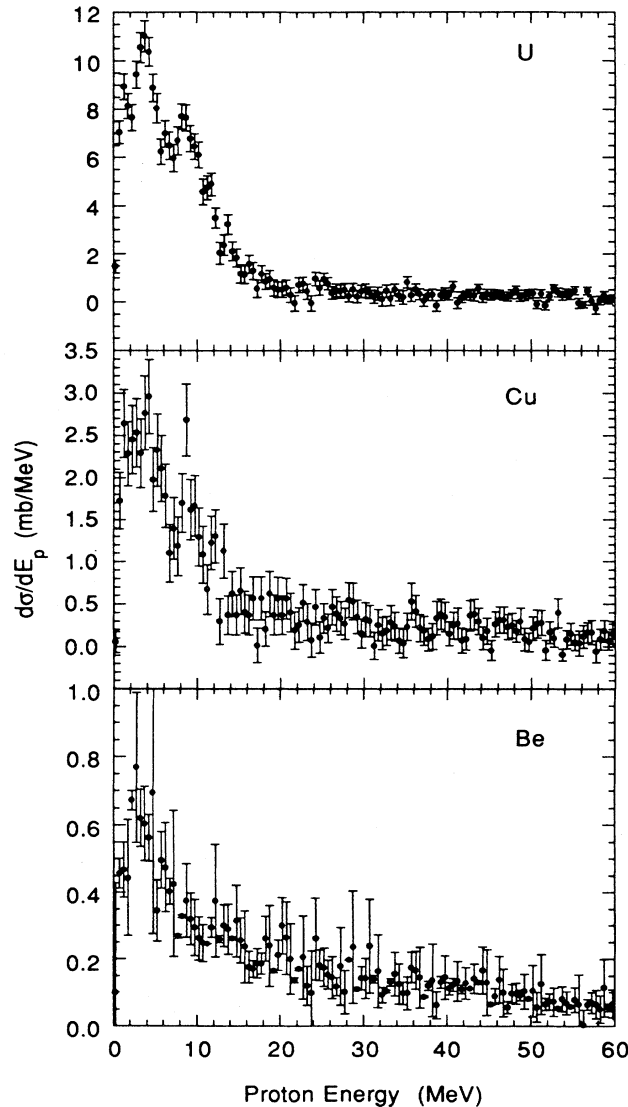


FIG. 2. The measured exclusive fragmentation cross section as a function of proton energy for U, Cu, and Be targets. The proton energy is measured in the projectile-fragment rest frame.

The structure in the low-energy region will be the subject of the remainder of this discussion.

Webb *et al.* attributed the low-energy peak seen in the  $^{12}\text{C}(^{12}\text{C}, ^{11}\text{B}+p)X$  and  $^1\text{H}(^{12}\text{C}, ^{11}\text{B}+p)X$  reactions to a combination of nucleon-nucleus ( $N-A$ ) diffractive scattering and an excitation process. For highly charged target nuclei, we expect a significant contribution resulting from the EMD process. It is clear from Fig. 2 that the low-energy cross section increases dramatically from Be to Cu to U. One can clearly see three peaks in the low-energy structure for the Cu and U targets, at 1.5, 4, and 9 MeV. The 4- and 9-MeV peaks are directly attributable to EMD. We attribute the 1.5-MeV peak to  $N-A$  diffractive scattering, which is most significant for the U target.

In our earlier studies of the EMD process [2, 16] we verified the applicability of the factorization of inclusive fragmentation cross sections to permit the separation of electromagnetic and direct nuclear processes. In the present work we extend this concept and assume that  $N-N$  diffractive scattering and the EMD process are incoherent. This assumption permits us to subtract the ( $N-N$ ) diffractive-scattering part of the cross section from the total cross section, leaving a combination of EMD and  $N-A$  diffractive scattering.

The method we have chosen to approximate the subtraction of the ( $N-N$ ) part is to subtract the measured cross section for the Be target, scaled appropriately, from that for the Cu and U targets. That is,

$$\frac{d\sigma_{\text{sub}}(\text{U})}{dE_p} = \frac{d\sigma(\text{U})}{dE_p} - \Gamma_U \frac{d\sigma(\text{Be})}{dE_p}, \quad (8)$$

where

$$\Gamma_U = \frac{\int [d\sigma(\text{U})/dE_p] dE_p}{\int [d\sigma(\text{Be})/dE_p] dE_p} \quad (9)$$

and the range of integration is  $30 < E_p < 50$  MeV. The scaling factors we derive are  $\Gamma_{\text{Cu}} = 1.82 \pm 0.25$  and  $\Gamma_U = 2.47 \pm 0.34$ . These are nearly equal to the values one expects from the target-radius dependence [16], which lends confidence to this procedure. The resulting  $d\sigma_{\text{sub}}/dE_p$  spectra for the U and Cu targets are shown in Fig. 3.

#### B. EMD and the $N-A$ component

After performing the subtraction described above we hypothesize that EMD and  $N-A$  diffractive dissociation are the only processes contributing to  $d\sigma_{\text{sub}}/dE_p$  and we assume that these processes do not interfere with each other. In this case, for the U target we get

$$\frac{d\sigma_{\text{sub}}(\text{U})}{dE_p} = \frac{d\sigma_{\text{em}}(\text{U})}{dE_p} + \frac{d\sigma_{NA}(\text{U})}{dE_p} - \Gamma_U \frac{d\sigma_{NA}(\text{Be})}{dE_p}. \quad (10)$$

We have applied the diffractive dissociation theory of Bertulani and Bauer [17] to describe the  $N-A$  diffractive dissociation cross sections,  $d\sigma_{NA}/dE_p$ .

For this we use Eq. (3.1) of Ref. [17] and identify the following quantities.  $Q$  is the magnitude of the three-

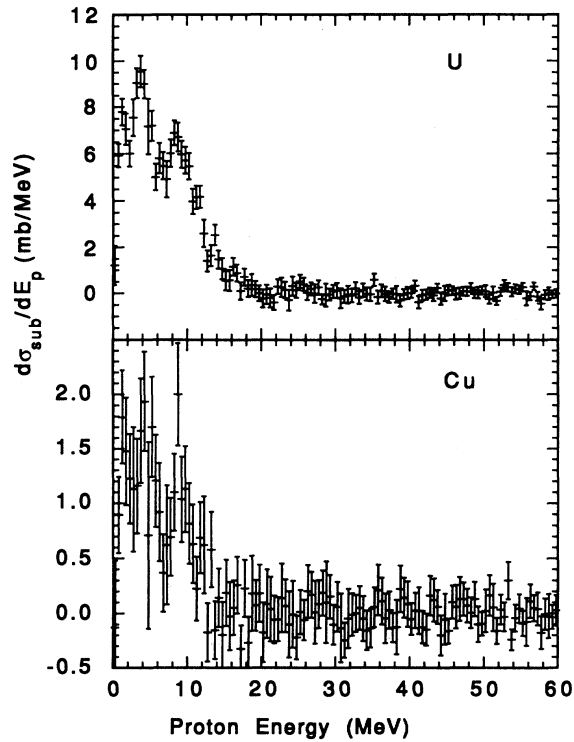


FIG. 3. The Be-subtracted cross sections ( $d\sigma_{\text{sub}}/dE_p$ ) for U and Cu targets.

momentum transfer,  $q$  is the momentum of the proton relative to the  $^{15}\text{N}$ , and  $R$  is the radius of the target nucleus. This experiment has good resolution for the relative momentum,  $q$ , but lacks resolution for the momentum transfer,  $Q$ . For our analysis we make the assumption that  $Q = q$  which implies that the momentum transfer in the diffractive dissociation process is completely absorbed by the proton. This is in agreement with the

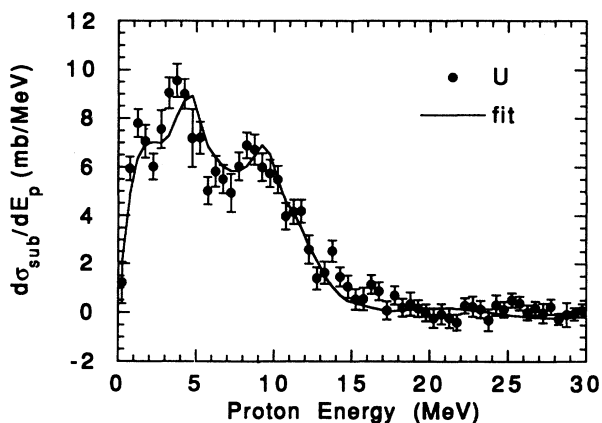


FIG. 4. The result of fitting Eq. (11) to the Be-subtracted U target cross section.

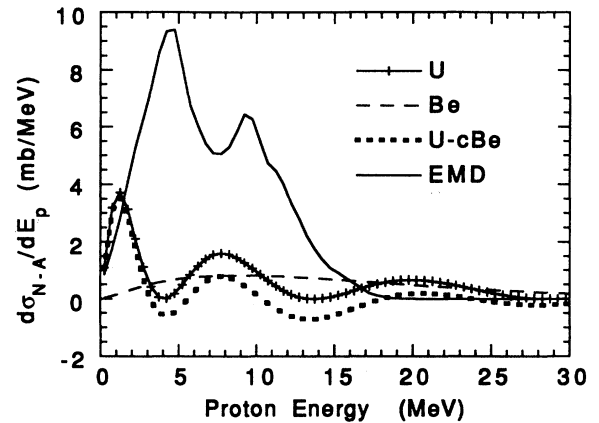


FIG. 5. The contributions of the different terms on the right-hand side in Eq. (11). EMD denotes first term, U denotes second term, Be denotes the third term, and U-cBe denotes combined second and third terms.

observations of Webb *et al.* [15].

Figure 4 shows the result of fitting the U target data with the following equation:

$$\frac{d\sigma_{\text{sub}}}{dE_p} = a \frac{d\sigma_{\text{em}}}{dE_p} + b \left( \frac{d\sigma_{NA}(R_U)}{dE_p} - \Gamma_U \frac{d\sigma_{NA}(R_{\text{Be}})}{dE_p} \right), \quad (11)$$

where  $a$ ,  $b$ , and  $R_U$  are the fitting parameters and we have set  $R_{\text{Be}} = 1.2A^{1/3} = 2.50$  fm. Figure 5 shows the contributions of the different terms in Eq. (11). The fit is insensitive to the radius for Be but the radius for the U target is important. The results of the fit are shown in Table I.

The normalization we have used for the cross sections would lead to the result of fit parameter  $a = 1$  if EMD would completely describe the cross section  $d\sigma_{\text{sub}}(U)/dE_p$ . The fitted value for  $a$  leads us to the conclusion that  $N$ - $A$  diffractive dissociation contributes about 8% to this cross section.

We expect that the value of  $R_U$  determined in this fit should agree with what one expects from the minimum impact parameter used for the EMD calculations (see Ref. [2]). The minimum impact parameter is calculated as  $b_{\text{min}} = R_{0.1}(\text{U}) + R_{0.1}(^{16}\text{O}) - d$ , where the overlap parameter  $d = -1.5$  fm is a result of Ref. [2]. If we naively associate half of the overlap with each nucleus,

TABLE I. Fit parameters from Eq. (11) for  $E_p < 30$  MeV.

Fitting results for the U target	
Parameter	Value
$a$	$0.915 \pm 0.019$
$b$	$(1.91 \pm 0.17) \times 10^{-2}$
$R_U$	$8.90 \pm 0.22$ fm
$\chi^2/\text{DOF}$	1.9

we get  $R_U = R_{0.1} + 0.75 \text{ fm} = 8.67 \text{ fm}$ . The agreement between this value and the result of fitting the present measurements verifies our assumption that  $d\sigma_{\text{sub}}/dE_p$  is the sum of EMD and  $N$ - $A$  diffractive dissociation.

The limited statistics for the Cu target data do not permit a detailed analysis as was performed for the U target data. However, the Cu cross section shown in Fig. 3 is consistent with the expected  $Z_T^{1.8}$  dependence [2] of the EMD process.

### C. $^{15}\text{N}$ decay $\gamma$ rays

The EMD theory predicts that the 9-MeV peak is due to excitation of the GDR in  $^{16}\text{O}$  followed by decay directly to the ground state of  $^{15}\text{N}$ , and that the 4-MeV peak results primarily from GDR decays to excited states in  $^{15}\text{N}$ .

As a consistency check of the EMD process we positioned a 49-element NaI detector at  $5^\circ$  relative to the beam direction (in the laboratory), which could detect  $\gamma$  rays from the decay of excited states in  $^{15}\text{N}$ . The solid angle acceptance of this detector was 5.5 msr (in the laboratory). With the kinematic focusing for 2.1A GeV fragments, this solid angle corresponds to a 1% acceptance for  $^{15}\text{N}$   $\gamma$  rays which are emitted isotropically.

Figure 6 shows the pulse-height spectrum we obtained with the NaI detector in coincidence with the  $^{16}\text{O} \rightarrow ^{15}\text{N} + p$  reactions. A 6.3-MeV  $\gamma$  ray from  $^{15}\text{N}$  gets Doppler shifted by a factor of 6 in the laboratory and therefore deposits about 38 MeV in the NaI detector. One sees that there is a broad structure in this range of the pulse-height spectrum. The energy calibration of the NaI detector was obtained from observation of cosmic-ray muons. This spectrum is shown in Fig. 7.

Figure 8 shows the  $^{15}\text{N} + p$  excitation energy spectrum for the U target with and without a requirement on the NaI pulse height. The solid circles represent those events in which the NaI detector registered a pulse in the range from 25 to 60 MeV. There is a clear peak at 4 MeV for

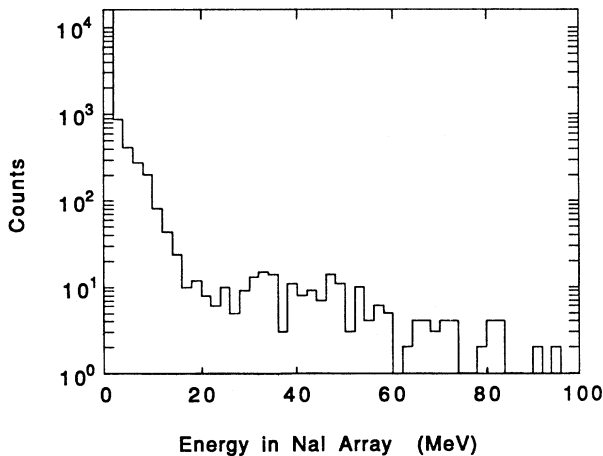


FIG. 6. Laboratory photon energy spectrum in the NaI detector for all  $^{15}\text{N} + p$  events.

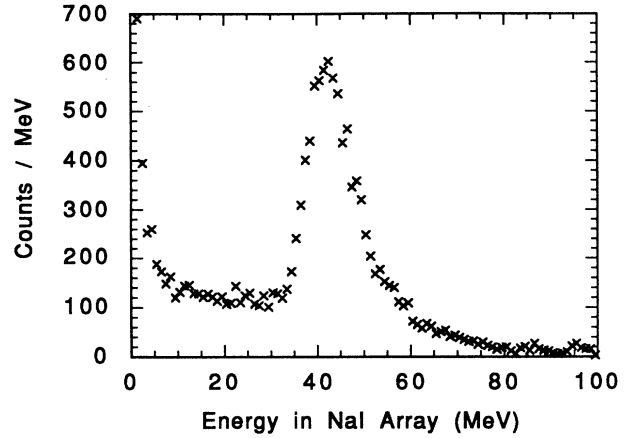


FIG. 7. The energy calibration spectrum for the NaI array using cosmic-ray muons. This corresponds to the energy deposited in one cell.

events with photons and a strong suppression of the 9-MeV peak. This is exactly what we expect for the EMD process.

## IV. CONCLUSIONS

We have measured the proton-energy spectra in the reaction  $T(^{16}\text{O}, ^{15}\text{N} + p)X$  for the targets ( $T$ ) U, Cu, and Be at 2.1A GeV. In agreement with Webb *et al.* [15] we find that there is a featureless high-energy tail for  $E_p > 20$  MeV, which we attribute to nucleon-nucleon quasielastic scattering. Below 20 MeV the cross section is dominated by the electromagnetic dissociation process,

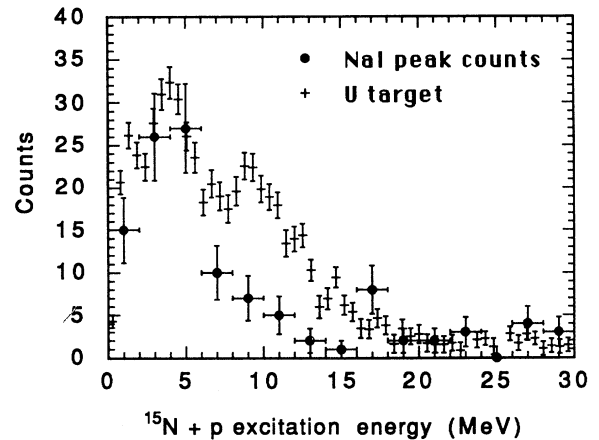


FIG. 8. The crosses show the total excitation energy spectrum for the U target and the solid circles the same spectrum from events for which the NaI detector registered a pulse between 25 and 60 MeV. The two curves are normalized to the same area for the 4-MeV peak. Note that the excitation energy is approximately 16/15 times the proton energy.

for high- $Z$  targets. An additional point of confirmation is the near absence of  $\gamma$  rays for events corresponding to the  $E_p=9$  MeV peak, because the 9-MeV peak results from the giant dipole resonance in  $^{16}\text{O}$  decaying directly to the ground state in  $^{15}\text{N}$ .

We have clearly demonstrated that nucleon-nucleus diffractive dissociation has a significant contribution (about 8% for the present case) to the cross section and must be considered in order to have a complete understanding of the differential cross section  $d\sigma/dE_p$ .

It has been pointed out many times [2, 18, 19] that application of EMD measurements to  $\beta$ -unstable nuclei would be very valuable for several reasons, not the least of which is that it would make possible the systematic delineation of the properties of the giant dipole resonance for nuclei ranging from one to several nucleons removed from the valley of  $\beta$  stability. The question has been whether beams of  $\beta$ -unstable nuclei could be produced that are intense enough to make possible such studies. In the present work, we had to reduce the  $^{16}\text{O}$  beam in-

tensity at the Bevalac from its normal value by a factor of  $\sim 10^5$  in order to achieve counting rates nearly free from pile-up. Thus, we have clearly shown with these exclusive cross-section measurements that the EMD process can be exploited to yield exciting possibilities for studying photonuclear reactions for both stable and  $\beta$ -unstable nuclei, and thus to open up a new and potentially very fruitful field of nuclear physics.

#### ACKNOWLEDGMENTS

We would like to thank Harry Heckman for his inspiring interest and pioneering efforts leading to this work. Additionally we would like to acknowledge many stimulating discussions with the late Abe Goldberg. This work was supported by DOE Contracts No. DE-AC03-76SF00098 and No. DE-FG05-86ER40285, NSF Grant No. PHY81-21003, and NASA Grant No. NGR-05-003-513.

\* Present address: Hoffman-LaRoche, Basel, Switzerland.

† Present address: Texas A&M University, College Station, Texas 77843.

- [1] H. H. Heckman and P. J. Lindstrom, *Phys. Rev. Lett.* **37**, 56 (1976).
- [2] D. L. Olson, B. L. Berman, D. E. Greiner, H. H. Heckman, P. J. Lindstrom, G. D. Westfall, and H. J. Crawford, *Phys. Rev. C* **24**, 1529 (1981).
- [3] L. Ramello, *Z. Phys. C* **38**, 73 (1987).
- [4] C. Brechtman and W. Heinrich, *Z. Phys. A* **330**, 407 (1988); **331**, 463 (1988); C. Brechtman, W. Heinrich, and E. V. Benton, *Phys. Rev. C* **39**, 2222 (1989).
- [5] P. B. Price, R. Guoxiao, and W.T. William, *Phys. Rev. Lett.* **61**, 2193 (1988).
- [6] I. Tanihata, *Nucl. Phys.* **A488**, 113c (1988).
- [7] J. Barrette, P. Braun-Munzinger, W. E. Clelend, G. David, E. Duek, M. Fatyga, D. Fox, S. V. Greene, J. R. Hall, R. Heifetz, T. K. Hemmick, N. Herrmann, R. W. Hogue, G. Ingold, K. Jayananda, D. Kraus, A. Legault, D. Lissauer, W. J. Llope, T. Ludlum, R. Majka, D. Makowiecki, S. K. Mark, J. T. Mitchell, M. Muthuswamy, E. O'Brien, L. H. Olsen, V. Polychronakos, M. Rawool-Sullivan, F. S. Rotondo, J. Sandweiss, B. Shivakumar, J. Simon, U. Sonnadara, J. Stachel, J. Sunier, H. Takai, T. G. Throwe, H. VanHecke, L. Waters, W. J. Willis, K. Wolf, D. Wolfe, and C. L. Woody, *Phys. Rev. C* **41**, 1512 (1990).
- [8] J. C. Hill, M. T. Mercier, F. K. Wohn, and A. R. Smith, *Phys. Rev. Lett.* **52**, 898 (1984); M. T. Mercier, J. C. Hill, F. K. Wohn, C. M. McCullough, M. E. Nieland, J. A. Winger, C. B. Howard, S. Renwick, and D. K. Matheis, *Phys. Rev. C* **33**, 1655 (1986); J. C. Hill, F. K. Wohn, J. A. Winger, and A. R. Smith, *Phys. Rev. Lett.* **60**, 999 (1988); J. C. Hill, F. K. Wohn, J. A. Winger, M. Khayat, K. Leininger, and A. R. Smith, *Phys. Rev. C* **38**, 1722 (1988); J. C. Hill, F. K. Wohn, J. A. Winger, M. Khayat, M. T. Mercier, and A. R. Smith, *ibid.* **39**, 524 (1989).
- [9] J. T. Caldwell, Ph.D. thesis, University of California, Report No. UCRL-50287 (1967).
- [10] J. T. Caldwell, S. C. Fultz, and R. L. Bramblett, *Phys. Rev. Lett.* **19**, 447 (1967).
- [11] J. E. E. Baglin and M. N. Thompson, *Nucl. Phys.* **A138**, 73 (1969).
- [12] R. C. Morrison, Ph.D. thesis, Yale University (1965).
- [13] J. Engelage, M. E. Baumgartner, E. Beale, B. L. Berman, F. Bieser, F. P. Brady, M. Bronson, J. B. Carroll, H. J. Crawford, I. Flores, D. E. Greiner, L. Greiner, O. Hashimoto, G. Igo, S. Kadota, P. N. Kirk, P. J. Lindstrom, C. McParland, S. Nagamiya, D. L. Olson, J. Porter, J. L. Romero, C. L. Ruiz, T. J. M. Symons, I. Tanihata, R. Wada, M. L. Webb, J. Yamada, and H. Yee, *Nucl. Instrum. Methods* **A277**, 431 (1988).
- [14] D. E. Greiner, P. J. Lindstrom, H. H. Heckman, Bruce Cork, and F. S. Bieser, *Phys. Rev. Lett.* **35**, 152 (1973).
- [15] M. L. Webb, H. J. Crawford, J. Engelage, M. E. Baumgartner, D. E. Greiner, P. J. Lindstrom, D. L. Olson, and R. Wada, *Phys. Rev. C* **36**, 193 (1987).
- [16] D. L. Olson, B. L. Berman, D. E. Greiner, H. H. Heckman, P. J. Lindstrom, and H. J. Crawford, *Phys. Rev. C* **28**, 1602 (1983).
- [17] C. A. Bertulani and G. Bauer, *Nucl. Phys.* **A480**, 615 (1988).
- [18] B.L. Berman, in *Proceedings of the Symposium on Perspectives in Electro- and Photonuclear Physics*, CEN Saclay, 1980 (unpublished), p. 7; B.L. Berman, in *Proceedings of the Workshop on Prospects for Research with Radioactive Beams from Heavy Ion Accelerators*, Washington, D.C., 1984 (unpublished), p. 92.
- [19] I. Tanihata, H. Hamagaki, O. Hashimoto, S. Nagamiya, Y. Shida, N. Yoshikawa, O. Yamakawa, K. Sugimoto, T. Kobayashi, D. E. Greiner, N. Takahashi, and Y. Nojiri, *Phys. Lett.* **160B**, 380 (1985); I. Tanihata, H. Hamagaki, O. Hashimoto, Y. Shida, N. Yoshikawa, K. Sugimoto, O. Yamakawa, T. Kobayashi, and N. Takahashi, *Phys. Rev. Lett.* **55**, 2676 (1985); I. Tanihata, Report No. RIKEN-AF-NP-58 (1987); *Nucl. Phys.* **A488**, 113c (1988).